

Mercury Cadmium Telluride (HgCdTe) pin Photodetector on Si/SOI Substrate

Salil Gupta¹, Jyoti Kedia²P.G. Student, Department of Electronics Engineering, PEC University of Technology, Chandigarh, India¹Assistant Professor, Department of Electronics Engineering, PEC University of Technology, Chandigarh, India²

ABSTRACT:The design of high performance detectors for optical communication system is a challenging task, so there is need for balance between absorption efficiency, wavelength ranges and cost which are to be overcome with suitable structure/design of the detectors. There is a need to study about the various parameters of the photodetectors and improve these parameters by modelling of Si based photodetectors, their compatibility with different materials. In order to improve the efficiency of the photodetector and as well as the cost, Hg_{1-x}Cd_xTe can be grown on Si/SOI substrate. In this thesis the HgCdTe pin MWIR photodetector is being integrated on the Si/SOI substrate and different parameters like dark current and quantum efficiency has been analysed, along with it the different curves have been plotted like the electric field profile, the net doping profile, energy band diagram, electrons and holes concentration inside the device. The quantum efficiency and dark current of the device on Si/SOI substrate has been compared with the values of the photodetector device on the conventional CdZnTe substrate and the results are quite comparable at the near room temperature. The quantum efficiency is nearly around 70-73% with SOI substrate and dark current is in the range of 10⁹A. The dark current is in the range of 10⁻²⁰A in case of silicon substrate with buffer layers which is very less and will lead to better efficiency of the device.

KEYWORDS: photodetectors, infrared, MWIR, pin, dark current, electric field, waveguide, silicon.

I. INTRODUCTION

The term photonics more specifically means the particle properties of light, the potential of creating signal processing device technologies using photons, the practical application of optics, and an analogy to electronics. Photonics is related to quantum optics, optomechanics, electro-optics, optoelectronics and quantum electronics. The term optoelectronics describes the devices or circuits that comprises with electrical and optical functions i.e., a thin-film semiconductor device. Nowadays the integrated photonic circuits are becoming popular in which the different optical devices are being integrated on a single chip to perform several optical communication applications. A photonic integrated circuit (PIC) or integrated optical circuit is a device that integrates multiple photonic functions and as such is similar to an electronic integrated circuit [1]. The major difference between the two is that a photonic integrated circuit provides functions for information signals imposed on optical wavelengths basically in the visible spectrum or near infrared spectrum. Unlike electronic integration where silicon is the dominant material, system photonic integrated circuits have been fabricated from a variety of material systems, including electro-optic crystals such as lithium niobate, silica on silicon, Silicon on insulator, various polymers and semiconductor materials which are used to make semiconductor lasers such as GaAs and InP [2] [3]. The different material systems are used because they each provide different advantages and limitations depending on the function to be integrated [4].

As the optical communication system is being integrated on a particular chip for performing particular functions, in order to meet the efficiency requirements of the system more stress is laid on the efficiency of the devices that are being integrated in a system. Since photodetection is major part of these photonic integrated devices, so there is a need to check and enhance the integrability of the photodetectors as well on this PIC platform. In every optical communication system the transmitter end i.e. laser, led and the receiver end i.e. photodetector are the most important components of the system for getting desired functioning of that system [5]. Photodetector is the device that is present at the receiver side in the photonics integrated system. So, with the development of PIC based products the development of the

International Journal of Innovative Research in Science, Engineering and Technology

(An ISO 3297: 2007 Certified Organization)

Vol. 5, Issue 7, July 2016

photodetectors speed for increase data rates is needed. For this majorly the integration of different materials with silicon is being carried out and the problems related to it because if the different materials which are used to manufacture photodetectors can give better efficiency when integrated with silicon, then this will result in better performance of photonics system on CMOS platform [6].

The light is incident on the device, the photons incident on the device should have energy more than the energy band gap of the material used for making the photodetector. These photons striking the active layer leads to the generation of electron and holes, the potential difference between the depletion layer produces electric field which directs the electrons and holes towards the anode and cathode generating respective currents. The luminescence is generated in the active region by the recombination of electrons that flow in from the n-type layer with holes that flow in from the p-type side. Any direct gap semiconductor can, in principle, be used for the active region, but in practice only a few materials are commonly employed. The main factors that determine the choice of the material are: the size of the band gap, constraints related to lattice matching, and the ease of p-type doping.

The materials like silicon, GaAs, germanium, InGaAs work on different wavelength ranges. Silicon works better in the wavelength range 0 to 1.1 μm , GaAs around 0.9 μm , Ge from 0.7 to 1.6, InGaAs from 0.9 to 1.8 μm [7][8]. This research work is concluded for particular infrared radiation range. Infrared detectors work in all ranges i.e. SIR, MWIR, LWIR and VLWIR [9] [10].

There are different types of photodetector like PIN, APD, MSM, Scottky and waveguide photodetectors but in this paper the stress has been laid on the pin photodetector. The infrared photodetector with pin structure has been integrated on Si/SOI substrate in order to analyse the efficiency and reduce the cost of the infrared photodetector.

II. BASICS OF INFRARED DETECTION

Infrared detection can be understood as the reaction to the infrared radiation. IR region just starts where human eye stops seeing. The first IR region is called Near IR (NIR) or Short Wave IR (SWIR). In this region, Night Vision Googles (NVG) using image intensifier tubes (I2T) and some lasers (wavelength of 1.064 μm and 1.54 μm) are operated. Imaging principles in the NIR or SWIR region are basically similar to visible region because both regions use reflected rays for detection. On the other hand, radiated IR rays are detected in mid-wave IR (MWIR), long-wave IR (LWIR), very long-wave IR (VLWIR) and far IR [9]. A wide variety of IR detectors have been developed comprising different materials and device architectures. Most commercially available detectors can be classified as one of the following:

1. Photon detectors (Photodetectors)
 - Intrinsic detectors
 - Extrinsic detectors
 - Photoemissive detectors
 - Quantum well and quantum dot detectors
2. Thermal detectors
 - Bolometers
 - Pyroelectric detectors
 - Thermopiles
 - Thermocouples
 - Radiation Field detectors

The distinction between infrared photon and thermal detectors is given by the difference in their operating mechanisms. Photon detectors are based on semiconductor materials that absorb incident IR photon radiation. The absorbed energy results in optical excitation, generating electron-hole pairs and changing the overall charge carrier distribution within the semiconductor [10]. The rapid photon-carrier interaction is observed in an electrical output signal typically measured by the collected device current. Because the incident photon energy influences absorption, the photon detector response is wavelength dependent as illustrated in Figure 1 (a), (b) [11].

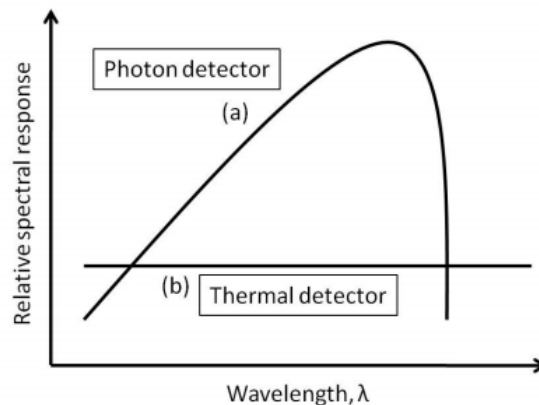


Figure 1: Generic (a) photon (b) thermal detector spectral response.

2.1 Low Bandgap Semiconductor Photodetectors

In order to sense IR radiation in the MWIR and LWIR spectral regions, low energy bandgap materials are used. Most widely used of these kinds of semiconductors are HgCdTe, InSb and InAsSb [12] [13].

Hg_{1-x}Cd_xTe (Mercury Cadmium Telluride-MCT): It is one of the most important semiconductors for IR detection. HgCdTe is a direct bandgap material. Its absorption coefficient is very high which provides high quantum efficiency. The 'x' represents CdTe mole fraction in the HgCdTe alloy. Cut-off wavelength of HgCdTe can be adjusted from 0.7 to 20 μ m by changing the CdTe mole fraction.

InSb (Indium Antimonide): It is an III-V compound semiconductor. InSb is an important semiconductor for the detection of IR in the MWIR region. The cut-off wavelength is 5.5 μ m at 77 K. Like HgCdTe, it is a direct bandgap material. Since InSb has high electron mobility, it has been used in IR imaging systems, magneto-resistive sensors, high-speed photodetectors and free space communication. InSb has strong covalent bonding, and large area InSb wafers (128x128, 256x256 etc.) are commercially available for MWIR applications [14].

In_{1-x}As_xSb (Indium Arsenide Antimonide): It is a ternary alloy for MWIR and LWIR applications. InAsSb is a direct bandgap material and its bandgap can be changed by varying the antimony mole fraction (x). The cut-off wavelength is tunable from 3.1 μ m ($x = 0.0$) to 9.0 μ m ($x \approx 0.6$). The longest cut-off wavelength of InAsSb is 9 μ m at 77 K. High quality InAsSb photodetectors for MWIR region have been developed during the last decades [15].

III. MODELING APPROACH

The objective of this research is to investigate the detector performance and sensitivity limiting mechanisms excluding the fabrication process related (generated) dark current/noise contributions. It should be noted that exact calculation of the HgCdTe detector performance under a specific combination of material composition and operating conditions is not possible even with numerical techniques due to insufficient and scattered information on some material parameters such as the trap levels, capture cross sections and carrier lifetimes, as well as field dependent transport properties. Therefore, the simulator of this work is constructed with the objective of observing the trends and the relations which would serve as a design guide for these sensors. While the geometrical effects can be modelled through 2D and 3D simulations, the main objective of this paper is to identify the relation between the intrinsic material parameters and the processes and the detector characteristics. Therefore, we constructed a 1D simulation which is reasonably compatible with the above described objectives.

International Journal of Innovative Research in Science, Engineering and Technology

(An ISO 3297: 2007 Certified Organization)

Vol. 5, Issue 7, July 2016

Great progress can be made in high quality crystal growth on mismatched substrates through use of planar optimization techniques, such as the appropriate choice of “buffer” layers, (sometimes with graded composition or superlattice structure), multiple growth rates and temperatures, and stress relaxation anneals. The approach which is followed that HgCdTe photodetector grown on Si Substrate instead of conventional CdZnTe substrate because of its high cost and simulated using the device modelling software ATLAS by Silvaco International. An additional planar approach is the use of Silicon-on-Insulator (SOI) substrates [16]. Such substrates provide an additional mode of strain relaxation via the relatively compliant, non-crystalline silicon dioxide. The comprehensive strategy for dislocation reduction includes the most effective planar optimizations for a particular material system, and the addition of nanopatterning, to work toward the best possible crystal growth on Si. Thus, the photodetector is simulated and its parameters are analysed with different values of x in $Hg_{1-x}Cd_xTe$ and there will be a buffer layer of the material CdZnTe which will be added between the intrinsic material and the silicon substrate. The major challenge which this design face is the threading dislocations. Crystal growth on lattice mismatched substrates (such as growth of HgCdTe on Si) leads to misfit dislocations at the interface between the substrate and grown layer. These result in threading dislocations (TDs) that can “thread” up to the top surface of the layer [17]. So, the parameters like responsivity, dark current, dynamic resistance are measured and the quantum efficiency of the photodetector will be analysed by simulation results.

The different values required for the simulation of the HgCdTe photodetectors have been calculated manually using the formulas mentioned below [18] [19] [20] [21]:

The intrinsic carrier concentration is given by:

$$n_i = (5.585 - 3.820x + 1.753 \times 10^{-3}T - 1.364 \times 10^{-3}xT) \times 10^{14} E_g^{3/4} T^{3/2} \exp(-E_g/2kT) \text{cm}^{-3} \quad (1)$$

Where ‘ x ’ is the cadmium mole fraction, T is the temperature and E_g is the bandgap. As we can see the intrinsic carrier concentration (n_i) does depend on the mole fraction as well as the temperature. The expression for the bandgap is given by:

$$E_{(x,T)} = -0.302 + 1.93x + 5.35 \times 10^{-4} T(1-2x) - 0.810x^2 + 0.832x^3 \quad (2)$$

where ‘ x ’ is the cadmium mole fraction and T is the temperature. It is a well known fact that the bandgap of HgCdTe can be tuned by changing the mole fraction. The temperature too plays a role in changing the bandgap. The fact that the bandgap can be changed allows us to access the narrow bandgap properties and the wide bandgap properties that the material can offer. The electron effective mass is given by:

$$m_n^* = \frac{1}{-0.6 + 6.333 \left(\frac{2}{E_g} + \frac{1}{E_g + 1} \right)} \quad (3)$$

where, E_g is the bandgap. The hole mass m_p^* is given as $0.55m_0$. HgCdTe is characterized by very low electron effective mass when compared to the hole effective mass. This in many ways shapes the way the device behaves. Since the electron mass is so low, the electrons also tend to have a very high mobility when compared to the holes. The current responsivity (R) of the photodetector is given as:

$$R = \frac{\eta q \lambda}{hc} \quad (4)$$

International Journal of Innovative Research in Science, Engineering and Technology

(An ISO 3297: 2007 Certified Organization)

Vol. 5, Issue 7, July 2016

IV. SIMULATIONS RESULTS AND DISCUSSION

In this the pin HgCdTe photodetector on conventional CdZnTe substrate has been designed and obtained results. In order to reduce the cost of the photodetector and also maintaining the parameter characteristics Si/SOI substrate is used. The design of the HgCdTe photodetector on silicon substrate will also help in integration of this infrared photodetector on CMOS platform. Mercury Cadmium Telluride (HgCdTe) is one of the most prominent semiconductor material for mid (2–5 μm) and long-wavelength (8–12 μm) infrared photon detectors. One of the promising approaches to achieving higher operating temperature infrared photon detectors was first proposed by [22] which was based on minority-carrier extraction and exclusion techniques under non-equilibrium condition. A two-dimensional numerical simulation of an HgCdTe infrared detector was carried out using ATLAS software.

Table 1 shows the structure being analysed with different mole fractions and the results have been obtained for dark current, quantum efficiency and electric field. By comparing the results from the table it can be said that the structure with the composition ($x=0.36, 0.26, 0.26$) gives the better dark current i.e. less than the other two compositions and also the quantum efficiency is better in this case along with the electric field values. The electric field values should be large so that there will be large drift in the electrons, generating more current. So this compositions has been taken for further analyses in next sections.

Table 1: Structures analysed with different mole fraction.

Structure	HgCdTe pin photodetector on SOI substrate($x=0.36, 0.26, 0.26$)	HgCdTe pin photodetector on SOI substrate with ($x=0.41, 0.35$ and 0.35)	HgCdTe pin photodetector on SOI substrate with ($x=0.31, 0.22$ and 0.22)
Dark current	6×10^{-9} A	8×10^{-9} A	4×10^{-6} A
Quantum efficiency	70-73 %	70-73%	60-65%
Electric Field	0.8×10^4 and 1.4×10^4 V/cm	0.8×10^4 and 1.3×10^4 V/cm	0.6×10^4 and 1.4×10^4 V/cm

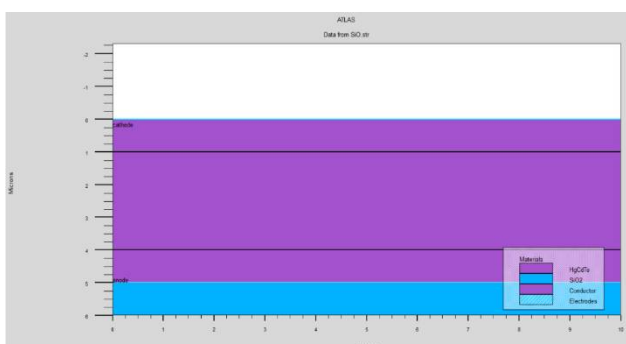


Figure 2(a): Structure of HgCdTe on SOI substrate electrodes.

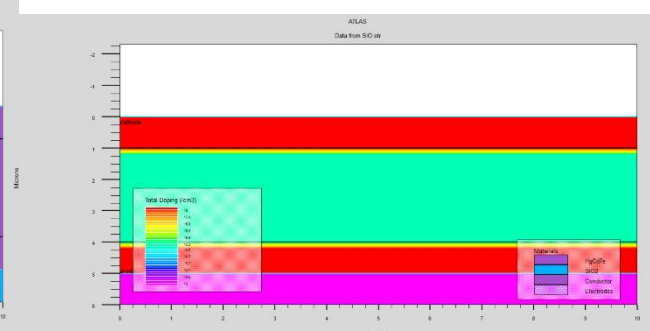


Figure 2(b): Structure of the device with net with doping.

4.1 HgCdTe Pin photodetector on SOI substrate at near room temperature

MCT is the best solution for single- and multiband systems covering a wide range of detection wavelengths because it is possible to tune the wavelength by selecting the appropriate composition. Detectors are usually hybridized to Si multiplexing circuits with indium interconnects and the hybrid cooled to operating temperatures in the region of 80 K. In this case we have simulated a pin HgCdTe photodetector on SOI substrate with a thin SiO₂ layer.

International Journal of Innovative Research in Science, Engineering and Technology

(An ISO 3297: 2007 Certified Organization)

Vol. 5, Issue 7, July 2016

Based on composition (Mole fractions-0.36, 0.26, 0.26)

The composition of the material $n^+ \text{-Hg}_{0.64}\text{Cd}_{0.36}\text{Te}/n^0 \text{-Hg}_{0.74}\text{Cd}_{0.26}\text{Te}/p^+ \text{-Hg}_{0.64}\text{Cd}_{0.36}\text{Te}$ with following mole fraction is used. The structure of the device, with doping profile and with meshing are shown in the Figure 2 (a), (b) and (c). In this structure we have simulated a pin photodetector on SOI substrate by using the thickness of the n^+ region (region 1) and p^+ (region 3) region as 1 microns and the intrinsic (n^0 -region 2) region as 4 microns and the SiO_2 layer of 1 microns. The refractive indices of the materials used are 3.1, 3.4, 3.1, and 1.4 for n^+ region, n^0 region, p^+ region and SiO_2 layers. The doping concentrations of the regions are taken same as the above case i.e. $1e18$, $1e15$ and $1e18$ for region 1, 2 and 3 respectively. The dark current V-I characteristics has been extracted for the device shown in the Figure 3 with the value of 6×10^{-9} A for the reverse biased voltage of 0.5 V which is nearly similar to the actual values.

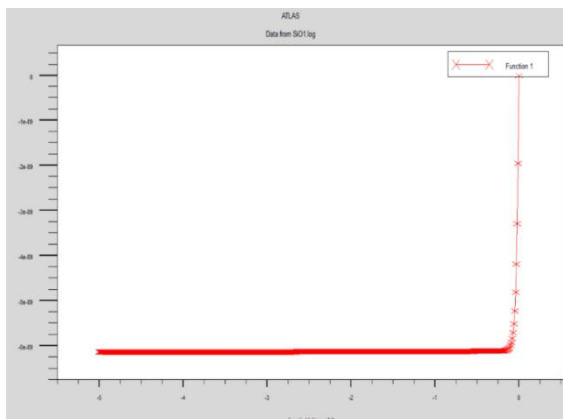


Figure 3: Dark current Characteristics

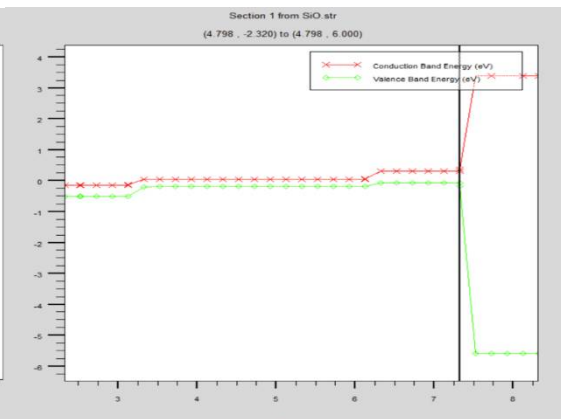


Figure 4: Conduction band energy and valence band energy.

Figure 4 shows the conduction band energy and the valence band energy of the device, the energy gap is around 0.4 eV which is comparable with the already extracted results [23].

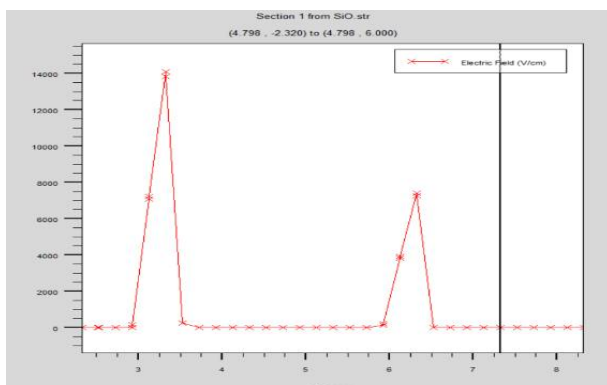


Figure 5: Electric field profile.

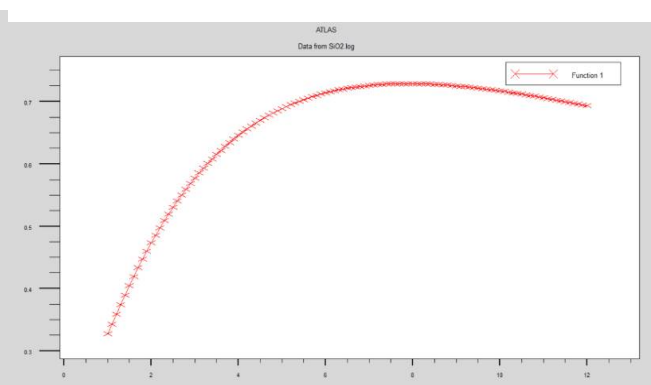


Figure 6: Quantum efficiency vs Optical wavelength for photodetector on SOI.

Figure 5 shows the the profile of the electric field $E(x)$ across the photodetector, in absence of infrared radiation flux. The electric field associated with the $n^+ \text{-Hg}_{0.64}\text{Cd}_{0.36}\text{Te}/n^0 \text{-Hg}_{0.74}\text{Cd}_{0.26}\text{Te}/p^+ \text{-Hg}_{0.64}\text{Cd}_{0.36}\text{Te}$ on SiO_2 layer gives a perfect triangular shapes of the maximum value 0.8×10^4 V/cm and 1.4×10^4 V/cm at $p^+ \text{-}n$ and $n \text{-}n^+$ metallurgical junctions of the structure respectively under equilibrium condition. The applied voltage drops across the metallurgical junction. The simulated result of electric profile shows that electric field is of negligible value within lightly doped

International Journal of Innovative Research in Science, Engineering and Technology

(An ISO 3297: 2007 Certified Organization)

Vol. 5, Issue 7, July 2016

neutral n-region under zero bias condition. Figure 6 shows the quantum efficiency of the structure which is 70-73%, that is slightly less than the above case. However, even if the quantum efficiency is less than in normal case the device on SOI substrate will work efficiently and will be cheaper than the conventional HgCdTe photodetector on CdZnTe substrate which will help in various applications.

Based on composition (Mole Fractions- 0.41, 0.35, 0.35)

Now for the different compositions of the HgCdTe the respective parameters have been analysed by changing the mole fraction (x) of the material, the structure now becomes $n^+ \text{Hg}_{0.59}\text{Cd}_{0.41}\text{Te}/n^0 \text{Hg}_{0.65}\text{Cd}_{0.35}\text{Te}/p^+ \text{Hg}_{0.65}\text{Cd}_{0.35}\text{Te}$ [19].

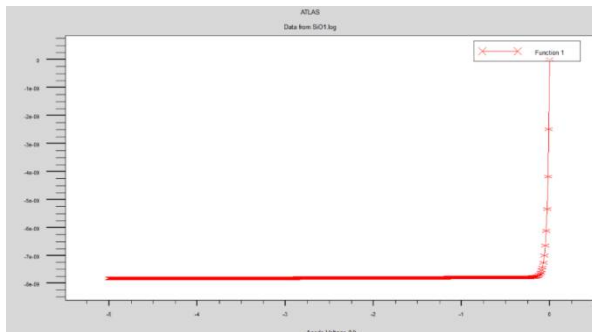


Figure 7: Dark current characteristics with mole fraction (0.31, 0.22 and 0.22)

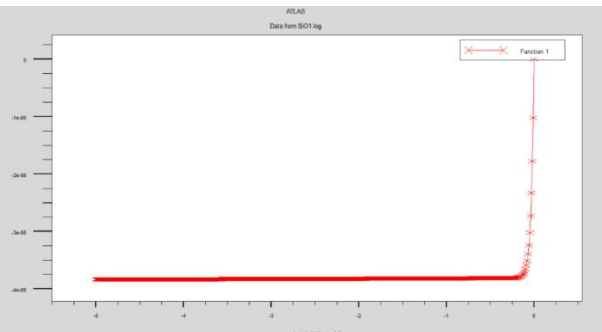


Figure 8: Dark current characteristics with mole(0.41, 0.35 and 0.35)

The quantum efficiency of this structure does not change with respect to the previous compositions but dark current slightly changes to 8×10^{-9} A, the dark current characteristics is shown in the Figure 7.

Based on composition (Mole fraction-0.31, 0.22, 0.22)

When the structure is being designed with composition of materials becomes $n^+ \text{Hg}_{0.69}\text{Cd}_{0.31}\text{Te}/n^0 \text{Hg}_{0.78}\text{Cd}_{0.22}\text{Te}/p^+ \text{Hg}_{0.78}\text{Cd}_{0.22}\text{Te}$ [20] the parameters we get are shown in Figure 8. The dark current value is 4×10^{-6} A and the quantum efficiency is around 60-65% which is less than the above cases as shown in Figure 9.

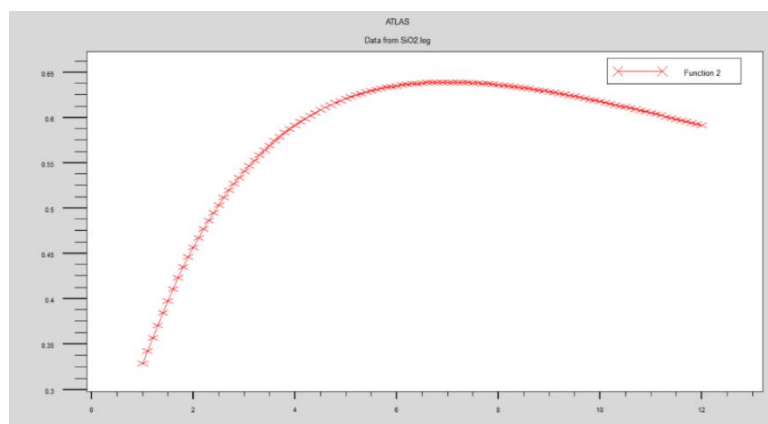


Figure 9: Quantum efficiency with mole fraction (0.31, 0.22 and 0.22).

4.2 HgCdTe pin Photodetector on Silicon Substrate with CdTe and ZnTe Buffer Layers

Hg_{1-x}Cd_xTe (MCT) is the material of choice for many infrared focal plane array applications. Low leakage and high carrier mobilities result in detectors with excellent sensitivity. MCT is the best solution for single- and multiband systems covering a wide range of detection wavelengths because it is possible to tune the wavelength by selecting the appropriate composition. The early efforts to grow MCT devices on Si involved growing CZT buffer layers by molecular beam epitaxy (MBE) for liquid phase epitaxy (LPE) MCT growth. The majority of MOVPE success has been on CZT and GaAs substrates. This has progressed to MCT growth on GaAs layers grown on Si, but poor morphology and reproducibility has so far prevented this from becoming a viable route. MBE growth of MCT has been reported on various Si substrate orientations [16]. As shown in the paper [16] a thin ZnTe buffer layer was grown by MBE to set the substrate orientation to (100) and improve the CdTe adhesion.

The structure which has been simulated in ATLAS by Silvaco is shown in Figure 10 where n⁺-Hg_{0.64}Cd_{0.36}Te/n⁰-Hg_{0.74}Cd_{0.26}Te/p⁺-Hg_{0.64}Cd_{0.36}Te is integrated on the silicon substrate with the buffer layers in between, CdTe layer with 2 microns thickness and ZnTe layer 1 micron thickness. The active region (absorption layer) in this structure is of 3 microns thickness, the anode and cathode placement is shown in the figure.

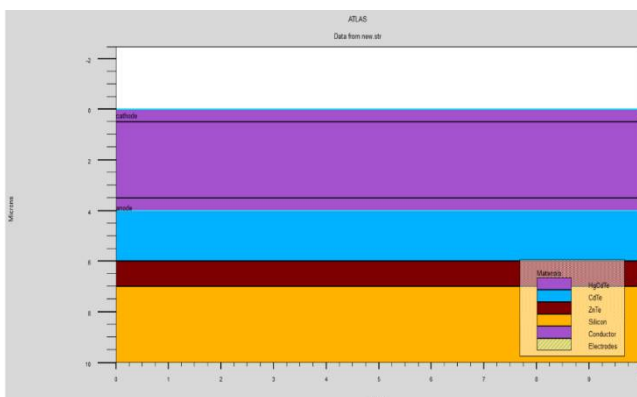


Figure 10: HgCdTe structure on silicon substrate. with buffer layers

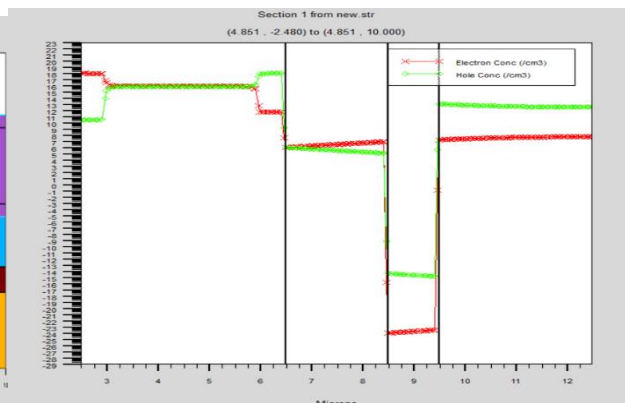


Figure 11: Electrons and holes concentration generated in the device.

The net doping of the layers of HgCdTe in the structure and the light beam of intensity 10⁻⁴ falling on the absorption layer over the surface. The contours have been shown in the form of net doping in the device structure. The doping variations is shown in the left corner of the structure diagram. The layers and the electrodes placement is also shown in the figure below on the right most corner at the bottom of the structure diagram. The region 1 is of 0.5µm, the region 2µm has thickness 3µm, the CdTe layer has the thickness of 2µm, the ZnTe has the thickness of 1µm and the silicon substrate layer has thickness of 3 µm.

When light (photons) falls on the device, if the energy of the photons is greater than the energy band gap of the device then it breaks the bonds and electron, holes are generated which further move towards anode and cathode under the influence of the electric field lead to the generation of anode and cathode current. Figure 11 shows the electron and holes concentration in the device. Electric field due to the potential difference between the depletion region and n or p side of the photodetector leads to the flow of electrons and holes in the device which gives rise to the current in the device. Figure 12 shows the electric field across the device structure. The electric field associated with the n⁺ Hg_{0.64}Cd_{0.36}Te/n⁰ Hg_{0.74}Cd_{0.26}Te/p⁺ Hg_{0.64}Cd_{0.36}Te on ZnTe/CdTe/Silicon gives maximum values of 3x 10⁴ V/cm, 1.5x 10⁴ V/cm and 8x 10⁴ V/cm at n⁺-n, n-p⁺ and p⁺-CdTe interface layers.

When the current is generated in the device in absence of the light falling on it, and only under the reverse bias voltage is provided then the current generated at the anode side, i.e. anode current is known as dark current which can also be understood as the leakage current.

International Journal of Innovative Research in Science, Engineering and Technology

(An ISO 3297: 2007 Certified Organization)

Vol. 5, Issue 7, July 2016

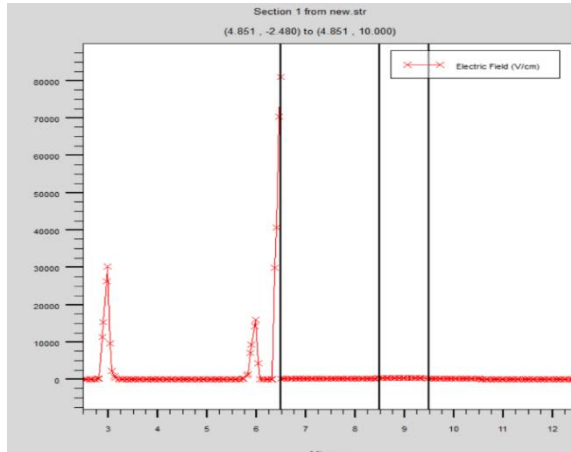


Figure 12: Electric field variations in the device structure

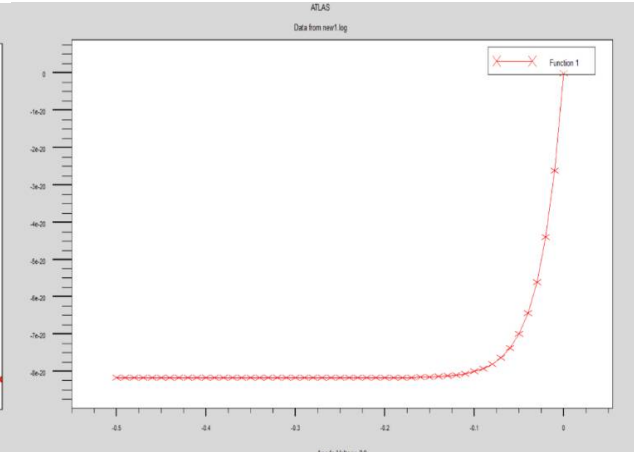


Figure 13: Dark current characteristics.

Figure 13 shows the dark current generated in the device shown above without the beam of light being incident. The dark current value which are obtained in this case is 8×10^{-20} A, which is very less and will lead to efficient working of the device because less dark current is desirable in the device. If the dark current will be less then there will be less deviation of the values from the actual theoretical value calculated.

Table 2: Different parameter values of the defined structures of HgCdTe.

Structure	HgCdTe pin photodetector results from research papers [23]	HgCdTe LWIR [24]	HgCdTe based MWIR photodetector or [21]	Normal HgCdTe pin photodetector	HgCdTe pin photodetector on SOI substrate(x=0.36, 0.26, 0.26)	HgCdTe pin photodetector on silicon with CdTe and ZnTe buffer layers
Dark current	1.8×10^{-8} A	10^{-7} A	-	10^{-9} A	6×10^{-9} A	8×10^{-20}
Quantum efficiency	-	-	~60%	~60% for MWIR, 77-78% for LWIR	70-73 %	-
Electric Field	-	0.5×10^4 and 0.45×10^4 V/cm	1.2×10^4 V/cm	1.5×10^4 and 3×10^4 V/cm	0.8×10^4 and 1.4×10^4 V/cm	3×10^4 , 1.5×10^4 and 8×10^4 V/cm

The results of the following structures are shown in the Table 2. The parameters of the HgCdTe photodetectors with composition $n^+ \text{Hg}_{0.64} \text{Cd}_{0.36} \text{Te} / n^0 \text{Hg}_{0.74} \text{Cd}_{0.26} \text{Te} / p^+ \text{Hg}_{0.64} \text{Cd}_{0.36} \text{Te}$ has been analysed and can be compared in the table give below. In this table there are results shown for 4 structures and parameters analysed i.e. the dark current, quantum efficiency and the electric field profile maximum values at the region interfaces. The HgCdTe pin photodetector on SOI substrate with different compositions have been analysed and the values for the parameters have been shown in the

International Journal of Innovative Research in Science, Engineering and Technology

(An ISO 3297: 2007 Certified Organization)

Vol. 5, Issue 7, July 2016

table. By this table we can say that the photodetector with the mole fraction ($x=0.36, 0.26, 0.26$) gives better results as the dark current is 6×10^{-9} A which is less than the other compositions and also the quantum efficiency is 70-73 % which is better among all the compositions. The electric field maximum values are almost similar in all the cases. So, these parameter values shows that the best composition for designing the photodetector is ($x=0.36, 0.26, 0.26$). The HgCdTe pin photodetector on silicon with CdTe and ZnTe buffer layers gives the dark current in the range of 10^{-20} A and the maximum values of the electric fields are 3×10^4 , 1.5×10^4 and 8×10^4 V/cm which will give more drift to the electrons and will result in larger current generation into the device.

V. CONCLUSION

This paper discusses the design and implementation of an HgCdTe photodetector device on Si/SOI substrate using ATLAS simulation software by Silvaco International. The primary aim of this thesis is to simulate key characteristics that determine the performance of an HgCdTe detector operating in the MWIR region. The device has been simulated in ATLAS assuming the various actual parameters and the desired results are being obtained on the near room temperatures. Mostly study has been done on 77K temperature for the HgCdTe, which is very low temperature to be maintained. So, the efficient working of device on 300K temperature is very essential in order to save the cost of designing. The integration of the HgCdTe photodetector on Si/SOI substrate instead of the conventional CdZnTe substrate will lead to cost reduction as well as more integratibility with photonic integrated circuits (PIC). The dark current for the device on SOI substrate is simulated to be 6×10^{-9} A, the quantum efficiency is analysed to be 70-73%, the other parameters like the energy band gap we get is 0.4 eV, the electric field profile is plotted with the maximum values of 0.8×10^4 and 1.4×10^4 at the interfaces between the regions. The quantum efficiency for the normal pin HgCdTe photodetector is also analysed and simulated to be 77-78 %. There is not much difference in the efficiency of the photodetector on SOI substrate which is less than the normal pin photodetector but still with 70-73% efficiency, the cost reduction can be considered as a large factor. The material structure has also been modified by integrating the pin HgCdTe on the silicon substrate by adding buffer layers of CdTe and ZnTe in order to decrease the lattice mismatch between the HgCdTe and the silicon. The dark current is extracted to be 8×10^{-20} A. The electric field profile is also plotted with the maximum values of 3×10^4 V/cm, 1.5×10^4 V/cm and 8×10^4 V/cm at n^+-n , $n-p^+$ and p^+-CdTe interface layers.

The results of the designed device are presented in terms of the dark current, quantum efficiency, electric field profile, electrons and holes concentration, energy band diagram, the net doping profile are also being plotted in TONYPLOT. The comparative study is demonstrated in the tabular form.

REFERENCES

- [1] Kartner F.X, Akiyama S., Byun H. et al., "Electronic photonic integrated circuits for high speed, high resolution, analog to digital conversion", proc. of SPIE, Vol. 6125, pp. 612503-1 - 14, 2006.
- [2] Rao M.V., Bhattacharya P.K., and Chen C.Y., "Low Noise In_{0.53} Ga_{0.47} As: Fe Photoconductive Detectors for Optical Communications," IEEE Trans. on Elect. Dep., vol. Ed-33, no. 1, pp .67-71, 1986.
- [3] R. Nagarajan *et al.*, "InP Photonic Integrated Circuits," in IEEE Journal of Selected Topics in Quantum Electronics, vol. 16, no. 5, pp. 1113-1125, Sept.-Oct. 2010.
- [4] Nejad H.E., Mir A., "Simulation and evaluation of PIN photodetectors based on materials and thickness of intrinsic layer," IEEE, pp 1078 - 1082, 2015.
- [5] Bogaerts W., Taillaert D., Luysaert B., Dumon P., Campenhout J., Bienstman P., Thourhout D., Baets R., Wiaux V., and Beckx S., "Basic structures for photonic integrated circuits in Silicon-on-insulator," Opt. Express 12, 1583-1591 (2004).
- [6] Kimerling L.C. et al., "Electronic-photonic integrated circuits on CMOS platform", Proc. of SPIE, Vol 6125, pp 612502 - 1-10, 2006.
- [7] Gao Y., Zhong Z., Feng S., "High Speed Normal Incidence p-i-n InGaAs photodetectors grown on silicon substrates by MOCVD," IEEE photonics technology letters, vol. 24, no. 4, pp 237 - 239, 2012.
- [8] Huang F.Y. et al., "Epitaxial SiGeC waveguide photodetector grown on Si substrate with response in the 1.3-1.55 μ m wavelength range," IEEE, vol. 9, No. 2, pp 229 - 231, February 1997.
- [9] Rogalski A., "Infrared Detectors: an overview," Infrared Physics & Technology, vol. 43, pp. 187-210, 2002.
- [10] Rogalski A. and Chrzanowski K., "Infrared devices and techniques," Opto-Electronics Review, vol. 10, pp. 111-136, 2002.
- [11] Marquis M., "Handouts on Thermal Imaging Systems Theory," Texas Instruments Incorporated Defense Systems, 1996.
- [12] Ashley T. and Elliott C.T., "Operation and properties of narrow-gap semiconductor devices near room temperature using non-equilibrium techniques," Semicond. Sci. Technol, vol. 6, pp. c99-c105, 1991.

International Journal of Innovative Research in Science, Engineering and Technology

(An ISO 3297: 2007 Certified Organization)

Vol. 5, Issue 7, July 2016

- [13] Ashokan R., Lee T.S., Zhao J., Chang Y., and Sivananthan S., "Mercury Cadmium Telluride For High Operating Temperature Infrared Detectors," Proceedings for the Army Science Conference, pp 1-8, 2004.
- [14] Nadimi M.,sadr A.," Simulation of Uncooled InSb Infrared Detectors", in Proc. IEEE, Int. Conf. on Modeling, Simulation and Control (ICMSC 2010), Cairo, Egypt, pp. 504-507, 2010.
- [15] Kimukin I., Biyikli N., Kartaloglu T., Aytur O. and Ozbay E., "High-speed InSb photodetectors on GaAs for mid-IR applications," in IEEE Journal of Selected Topics in Quantum Electronics, vol. 10, no. 4, pp. 766-770, July-Aug. 2004.
- [16] Hall D.J, Buckle L., Gordon N.T, Giess J., Hails J.E, Cairns J.W., Lawrence R.M., Graham A., Hall R.S., Maltby C., T. Ashley, "High-performance long wavelength HgCdTe infrared detectors grown on silicon substrates," Applied Physics Letters vol 85, no. 11, 2113-2115, 2004.
- [17] Peterson J.M., Franklin J.A, Reddy M., Johnson S.M, "High quality Large-Area MBE HgCdTe/Si," Journal of ELECTRONIC MATERIALS, Vol. 35, No.6, pp 1283-1286, 2006.
- [18] Dwivedi A.D.D, "Analytical modeling and atlas simulation of $p^+-Hg_{0.78}Cd_{0.22}Te/n-Hg_{0.78}Cd_{0.22}Te/CdZnTe$ homojunction photodetector for LWIR free space optical communication system," Journal of electronic devices, Vol 9, pp. 396-404, 2011.
- [19] Dwivedi A.D.D and Chakrabarti P., "Analytical modeling and numerical simulation of $Hg_{1-x}Cd_xTe$ based $n^+n^0p^+$ photodetector for MWIR free space optical communication", International Journal of advanced applied physics research, pp 20-27, 2015.
- [20] Dwivedi A.D.D and Chakrabarti P., "Analytical modeling and ATLAS simulation of $N^+-Hg_{0.69}Cd_{0.31}Te/n^0-Hg_{0.78}Cd_{0.22}Te/p^+Hg_{0.78}Cd_{0.22}Te$ p-i-n photodetector for long wavelength free space optical communication," Optoelectronics and advanced materials – rapid communications vol. 4, no. 4, p. 480 – 497, 2010.
- [21] Dwivedi A.D.D and Chakrabarti P., "Modeling and ATLAS simulation of HgCdTe based MWIR photodetector for free space optical communication", BHU, IEEE, pp 412-415, 2008.
- [22] Ashley T. and Elliott C.T., "Operation and properties of narrow-gap semiconductor devices near room temperature using non-equilibrium techniques," Semicond. Sci. Technol, vol. 6, pp. c99-c105, 1991.
- [23] Nadimi M. and Sadr A., "Modeling and simulation of high operating temperature MWIR photodetector based on Mercury Cadmium Telluride," International journal of Computer and Electrical Engineering, Vol. 3, No. 4, pp. 597-599, August 2011.
- [24] Saxena P.K and Chakrabarti P., "ATLAS Simulation of LWIR Photodetector based on HgCdTe", BHU, IEEE, pp. 427-430, 2007.
- [25] Velicu S., Badano G., Selamat Y., "HgCdTe/CdTe/Si Infrared Photodetectors Grown by MBE for Near-Room Temperature Operation," Journal of Electronic Materials, vol 30, No. 6, pp 711-716, 2001.
- [26] Velicu S., Grein C.H., Emelie P.Y., Itsuno A., Phillips J.D., and Wijewarnasuriya P.S., "MWIR and LWIR HgCdTe infrared detectors operated with reduced cooling requirements," J. Electron. Materials, vol. 39, no. 7, pp.873-881, 2010.
- [27] Yin D. et al., "High-Responsivity InGaAs/Inp Photodetectors Integrated On Silicon-On-Insulator Waveguide Circuits", 14th ICOCN, pp 1 – 3, 2015.
- [28] Hasim M R and Yusoff M.Z.M., "Modification and modeling of Ni/Si interface for photodetector applications," IEEE, pp 805 – 810, 2006.
- [29] Gammel J.C., Ohno H., and Ballantyne J.M., "High Speed Photoconductive Detectors Using InGaAs," IEEE J. of Quantum Elect., vol. QE-17, no. 2, pp. 269–272, 1981.
- [30] El_Mashade et al., "Characteristics Determination of Quantum Well Infrared Photodetectors," IEEE Mediterranean Microwave Symposium, pp. 29-40, 2003.
- [31] Chen Y. et al., "High performance long wavelength infrared HgCdTe focal plane arrays fabricated on CdSeTe compliant Si substrates," IEEE, vol. 57, No.4, 782 – 787, April 2010.
- [32] Carmody M., Yulius A., Edwall E. et al., "Recent progress in MBE growth of CdTe and HgCdTe on (211)B GaAs substrates," Journal of ELECTRONIC MATERIALS, Vol. 41, No. 10, pp 2719-2724, 2012.
- [33] Ashokan R., Lee T.S., Zhao J., Chang Y., and Sivananthan S., "Mercury Cadmium Telluride For High Operating Temperature Infrared Detectors," Proceedings for the Army Science Conference, pp 1-8, 2004.